

# Simulation of Multifilament Semicrystalline Polymer Fiber Melt-Spinning

Young-Pyo Jeon, Christopher L. Cox

Mathematical Sciences, Clemson University, Clemson, South Carolina, USA

Correspondence to:

Christopher L. Cox, email: [clcox@clemson.edu](mailto:clcox@clemson.edu)

## ABSTRACT

The goal of this effort is to provide an accurate simulation of multifilament fiber melt spinning, applicable for a wide range of material and process conditions. For ease of use, the model should run on a standard laptop or desktop computer in reasonable time (one hour or less). Most melt spinning models simulate the formation of a single filament, with little or no attention given to multifilament effects. Available multifilament simulations are primarily limited to Newtonian constitutive models for the polymer flow. We present a multifilament simulation based on the flow-enhanced crystallization approach of Shrikhande et al. [J. Appl. Polym. Sci., 100, 2006, 3240-3254] combined with a variant on the multifilament quench model of Zhang, et al. [J. Macromol. Sci. Phys., 47, 2007, 793-806]. We demonstrate the versatility of this model by applying it to isotactic polypropylene and polyethylene terephthalate, under a variety of process conditions. Key words: Computer modeling; Semi-crystalline polymer; Multifilament; Melt-spinning.

## INTRODUCTION

Fiber melt spinning is one of the most common industrial polymer processes. In multifilament spinning, the molten polymer exits from a forming die, or spinneret, into the quench zone where cooling air is blown across fibers (often numbering in the thousands) and the fibers solidify as they cool and are stretched (see *Figure 1*). Extreme changes in process conditions (e.g. temperature and axial velocity) occur during this stage resulting in large changes in fiber properties at the macro level (diameter, temperature) and molecular or structure level (polymer orientation, degree of crystallinity for semi-crystalline polymers). Quench conditions strongly influence the structure, which is directly linked to final properties. Experimental data confirm that variations in quench properties across a multifilament bundle create nonuniformities in fiber properties [1].

Predictive models have the ability to provide a

clearer understanding of the fiber spinning process, allowing both troubleshooting for existing systems and improved process design. Examples along with a review of early fiber spinning models can be found in [2]. Simulations of multifilament spinning of PET fibers, based on a Newtonian constitutive model, are described in [3], [4], and [5].

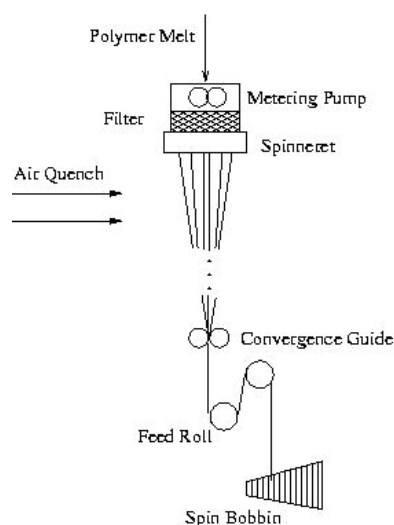


FIGURE 1. Schematic of fiber spinning process

Most commodity polymers are semi-crystalline, meaning that both crystalline and amorphous regions exist together in the solid state. Flow-enhanced (flow-induced, or stress-induced) crystallization is known to occur as a result of high tensile stresses in the fibers. One of the more recent FEC models is the one developed by McHugh, et al [6-9]. Their experimentally validated approach, which combines a viscoelastic constitutive model for the melt with a rigid rod model for the crystalline phase, is able to predict the location along the spinline of the necking phenomenon associated with rapid phase change under high-stress conditions.

Harvey and Doufas recently published results of a multifilament simulation coupling a single filament model with a 3D solution for the quench domain based on the Navier Stokes equations [10]. Their code requires extensive computing resources (both time and memory) and no experimental validation of results have been reported.

The authors of the current manuscript combined the FEC model in [9] with the multifilament quench model in [4], resulting in a simulation which compares favorably to industry data for PET multifilament spinning and also runs on a standard personal computer in minutes rather than hours [11]. This model includes viscoelastic effects and semicrystalline behavior in a nonisothermal multifilament setting.

The purpose of this paper is to describe a variation of the multifilament fiber melt-spinning model in [11], motivated by the work of Zhang et al. [5]. The simulation is applied to two polymers which differ significantly in their characteristics during processing. The rest of this paper is organized as follows. In the next section, the governing equations for the fibers and quench environment are developed. Simulation results are then provided for a variety of process conditions. The paper concludes with a summary and an outline of continuing work.

### GOVERNING EQUATIONS

The McHugh FEC model accurately predicts effects of viscoelasticity and phase change for a melt-spun fiber [9]. We encapsulate the FEC equations for a single fiber within a simple algorithm which accounts for convective heat transfer between the quench air and the fibers. The conservation equations for the quench environment, in discrete form, are similar to those in [4] and [5]. The overall algorithm is illustrated in *Figure 2*.

In this section we provide a brief description of the FEC model and a more detailed discussion of the equations governing the quench air.

#### FEC Fiber Spinning Model

The 1D FEC model assumes that all dependent variables (axial velocity ( $v_z$ ), temperature ( $T$ ), conformation tensor components ( $c_{zz}$  and  $c_{rr}$ ), semicrystalline orientation tensor component ( $S_{zz}$ ), and relative degree of crystallization ( $x$ )), depend only on  $z$ , the axial distance. Fiber diameter,  $D$ , can be calculated based on mass conservation (with mass flow rate,  $W$ , assumed constant). The fiber is also assumed to be at steady-state with constant density,  $\rho$ . Acceleration,  $dv_z/dz$ , is also a dependent variable so

that the system of equations forms a set of first-order ordinary differential equations. A full development of the FEC model can be found in the papers of McHugh, et al. [6-9]. We focus on aspects of this model most pertinent to temperature dependence and heat transfer.

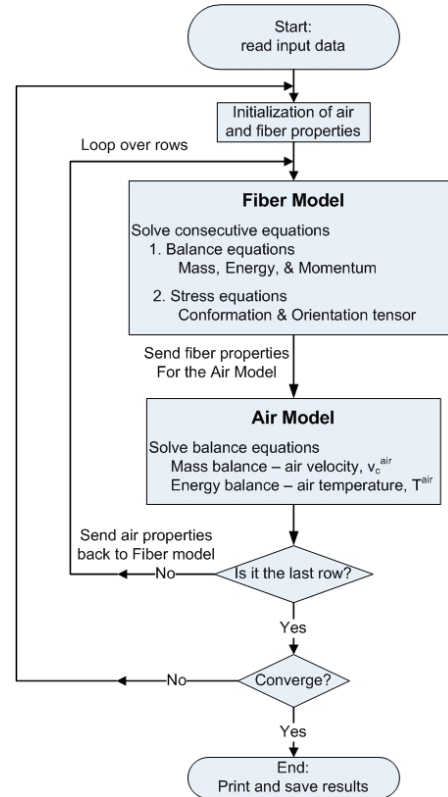


FIGURE 2. Overview of multifilament simulation

The zero-shear-rate viscosity of the melt used in our version of the model takes the form of the Arrhenius equation,

$$\eta_0(T) = \eta_A \exp\left(\frac{\eta_B}{T}\right) \quad (1)$$

The FEC model uses the empirical heat transfer coefficient of Kase and Matsuo [12] in the form

$$h_c = 0.42k \left(\frac{v_z}{D^2 \mu^{air}}\right)^{1/3} \left[1 + \left(\frac{8v_c^{air}}{v_z}\right)^2\right]^{1/6} \quad (2)$$

in which  $k$  is heat conductivity,  $\mu^{air}$  is air viscosity, and  $v_c^{air}$  is cross-flow quench air velocity. The

conservation of energy equation for the fiber takes the form

$$v_z \frac{dT}{dz} = C_1(D, v_z) h_c (T - T^{air}) + C_2(v_z, \frac{dv_z}{dz}, c_{zz}, c_{rr}, x) \quad (3)$$

where  $C_1$  and  $C_2$  are coefficients that depend on solution variables, as indicated, and material parameters. This equation plays a central role in coupling the quench and fiber models. The momentum equation has an air drag term which also couples the two models, normally in a less significant way. Specific details about the governing equations for the fiber model can be found in [6-9].

The numerical solution of the FEC equations for a single fiber is accomplished using a shooting method. In this algorithm, all dependent variables except  $c_{zz}$  are set at the spinneret and a nonlinear system solver is used to iteratively determine the initial value of  $c_{zz}$  which results in a specified take-up speed at the feed roll.

### Multifilament Quench Model

The model we employ to simulate the multifilament quench environment is based on the work of Dutta [4] and Zhang et al. [5], consisting of conservation equations for mass and energy. We assume that all fibers in a row transverse to the quench air cross-flow experience the same air velocity and temperature, and that the fibers are arranged in a rectangular array as shown in Figure 3.

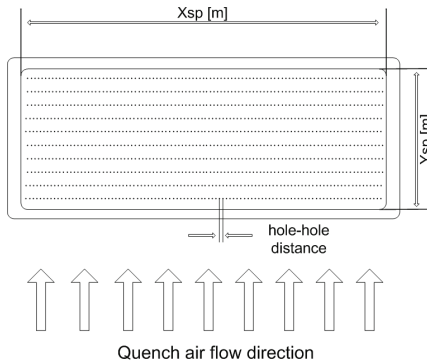


FIGURE 3. Spinneret geometry

Consider the computational cell in Figure 4 for one filament cross-section.

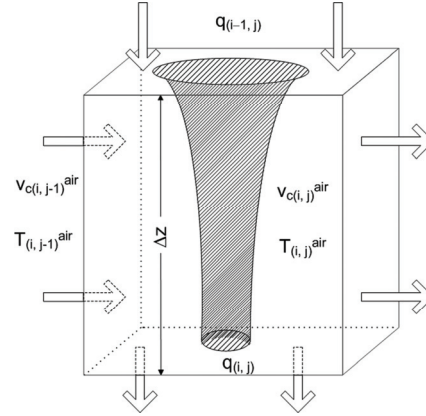


FIGURE 4. A schematic diagram of a computational cell containing a filament cross-section.

A mass balance on cell (i, j) using the notation in Figure 3 takes the form

$$(\rho^{air} v_c^{air} A_c)_{(i,j-1)} + q_{(i-1,j)} = (\rho^{air} v_c^{air} A_c)_{(i,j)} + q_{(i,j)} \quad (4)$$

where  $\rho^{air}$  is the air density,  $v_c^{air}$  is air cross-flow velocity,  $q$  is the downward air mass flow rate, and  $A_c$  is the area of the cell border perpendicular to the primary direction of the quench air flow. Dutta calculates  $q$  using the equation

$$q = 2\pi\rho^{air} \int_{r_f}^{R_{eff}} r v_d dr \quad (5)$$

where  $r_f$  is the fiber radius,  $v_d$  is the downward air velocity, and  $R_{eff}$  is an effective radius for each fiber, defined in terms of the number of fibers,  $N$ , and the area of the spinneret,  $A_{sp}$ , as

$$A_{sp} = N\pi R_{eff}^2 \quad (6)$$

Dutta uses Matsui's expression for the downward air velocity [13]:

$$v_d = v_z \left\{ 1 - \int_{\psi}^1 \frac{C_D \cdot Re_D}{\psi + [\psi^2 + \lambda(1 - \psi^2)^2]^{1/2}} d\psi \right\} \quad (7)$$

where  $\Psi$  is a dimensionless radius ( $\Psi = \sqrt{r_f/r}$ ),  $Re_D$  is the Reynold's number ( $Re_D = D\rho v/\mu$ ),  $C_D$  is the drag coefficient ( $C_D = 1.22K^{0.78} Re_D^{-0.61}$  and  $K = 0.22$ ), and  $\lambda$  is a constant being related to Prandtl's mixing

length ( $\lambda = K^2 Re_D^2 C_D / 2$ ). Combining eqs. (5) and (7) gives a complete expression for the downward air mass flow rate,

$$q = -4\pi\rho^{air}r_f^2v_z \int_1^{\psi_{eff}} \frac{1}{\psi^s} \left[ 1 - \int_{\psi^s}^1 \frac{C_D \cdot Re_D}{\psi + [\psi^2 + \lambda(1-\psi^2)^2]^{1/2}} d\psi \right] d\psi^s \quad (8)$$

in which the dimensionless effective radius,  $\psi_{eff}$ , is defined as  $\psi_{eff} = \sqrt{R_{eff} / r_f}$ .

From the mass balance (4) imposed on each cell, we obtain quench air velocity,  $v_{c(i,j)}^{air}$ :

$$v_{c(i,j)}^{air} = \frac{v_{c(i,j-1)}^{air} \rho_{c(i,j-1)}^{air} A_{c(i,j-1)} - q_{(i,j)} - q_{(i-1,j)}}{\rho_{c(i,j)}^{air} A_{c(i,j)}} \quad (9)$$

The equation used for calculating the air temperature begins with consideration of the energy input and output for the computational cell in *Figure 4*, formulated by Dutta as the heat capacities of the poly-

$$E_{in} = WC_p T_{(i-1,j)} + \rho_{c(i,j-1)}^{air} v_{c(i,j-1)}^{air} A_{c(i,j-1)} C_{p(i,j-1)}^{air} T_{(i,j-1)}^{air} + 0.5q_{(i-1,j)} (C_{p(i-1,j-1)}^{air} T_{(i-1,j-1)}^{air} + C_{p(i-1,j)}^{air} T_{(i-1,j)}^{air}) \quad (10)$$

$$E_{out} = WC_p T_{(i,j)} + \rho_{c(i,j)}^{air} v_{c(i,j)}^{air} A_{c(i,j)} C_{p(i,j)}^{air} T_{(i,j)}^{air} + 0.5q_{(i,j)} (C_{p(i,j-1)}^{air} T_{(i,j-1)}^{air} + C_{p(i,j)}^{air} T_{(i,j)}^{air}) \quad (11)$$

$$E_{in} = WC_p T_{(i-1,j)} + \rho_{c(i,j-1)}^{air} v_{c(i,j-1)}^{air} A_{c(i,j-1)} C_{p(i,j-1)}^{air} T_{(i,j-1)}^{air} + \frac{2\pi\rho_{p(i-1,j)}^{air} C_{p(i-1,j)}^{air}}{e^{-r_{f(i,j)}} - e^{-R_{eff}}} \int_{r_f}^{R_{eff}} v_{d(i-1,j)} \left[ \left( e^{-10^k r} - e^{-10^k R_{eff}} \right) T_{(i,j)} + \left( e^{-10^k r_{f(i,j)}} - e^{-10^k r} \right) \frac{T_{(i-1,j-1)}^{air} + T_{(i-1,j)}^{air}}{2} \right] r dr \quad (12)$$

$$E_{out} = WC_p T_{(i,j)} + \rho_{c(i,j)}^{air} v_{c(i,j)}^{air} A_{c(i,j)} C_{p(i,j)}^{air} T_{(i,j)}^{air} + \frac{2\pi\rho_{p(i,j)}^{air} C_{p(i,j)}^{air}}{e^{-r_{f(i+1,j)}} - e^{-R_{eff}}} \int_{r_f}^{R_{eff}} v_{d(i,j)} \left[ \left( e^{-10^k r} - e^{-10^k R_{eff}} \right) T_{(i+1,j)} + \left( e^{-10^k r_{f(i+1,j)}} - e^{-10^k r} \right) \frac{T_{(i,j-1)}^{air} + T_{(i,j)}^{air}}{2} \right] r dr \quad (13)$$

Equating the right hand sides of eqs. (12) and (13) and solving for  $T_{(i,j)}^{air}$  results in

In (10) and (11),  $T^{air}$  is the air temperature, and  $C_p$  and  $C_p^{air}$  are

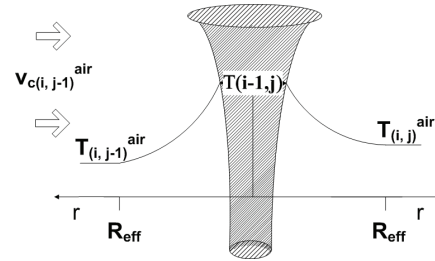


FIGURE 5. The air temperature distribution around fiber.

mer and air, respectively. Each is formulated as a polynomial in the respective temperatures [11]. As developed in Dutta [4], the three terms on the right hand sides of (10) and (11) represent heat due to the polymer, heat due the quench air flowing transversely, and heat due to the air pumped downwards, respectively.

Zhang, et al. modified Dutta's model by introducing an exponentially weighted distribution of temperatures, illustrated in *Figure 5*. We modify the form of the weighting term used in Zhang et al. in order to better control the weight given to the fiber temperature relative to the air temperature. Our variation on equations (10) and (11) is given by (12) and (13).

$$T_{(i,j)}^{\text{air}} = \left[ \begin{aligned} & WC_p [T_{(i-1,j)} - T_{(i,j)}] + \rho_{(i,j-1)}^{\text{air}} v_{c(i,j-1)}^{\text{air}} A_{c(i,j-1)} C_{p(i,j-1)}^{\text{air}} T_{(i,j-1)}^{\text{air}} \\ & + \frac{2\pi\rho_{(i-1,j)}^{\text{air}} C_{p(i-1,j)}^{\text{air}}}{e^{-10^k r_{f(i,j)}} - e^{-10^k R_{\text{eff}}}} \left[ \left( T_{(i,j)} - \frac{T_{(i-1,j-1)}^{\text{air}} + T_{(i-1,j)}^{\text{air}}}{2} \right) \int_{r_{f(i,j)}}^{R_{\text{eff}}} v_{d(i-1,j)} e^{-10^k r_{\text{rdr}}} + \left( \frac{T_{(i-1,j-1)}^{\text{air}} + T_{(i-1,j)}^{\text{air}}}{2} e^{-10^k r_{f(i,j)}} - T_{(i,j)} e^{-10^k R_{\text{eff}}} \right) \int_{r_{f(i,j)}}^{R_{\text{eff}}} v_{d(i-1,j)} r_{\text{rdr}} \right] \\ & - \frac{2\pi\rho_{(i,j)}^{\text{air}} C_{p(i,j)}^{\text{air}}}{e^{-10^k r_{f(i+1,j)}} - e^{-10^k R_{\text{eff}}}} \left[ \left( T_{(i+1,j)} - \frac{T_{(i,j-1)}^{\text{air}}}{2} \right) \int_{r_{f(i+1,j)}}^{R_{\text{eff}}} v_{d(i,j)} e^{-10^k r_{\text{rdr}}} + \left( \frac{T_{(i,j-1)}^{\text{air}}}{2} e^{-10^k r_{f(i+1,j)}} - T_{(i+1,j)} e^{-10^k R_{\text{eff}}} \right) \int_{r_{f(i+1,j)}}^{R_{\text{eff}}} v_{d(i,j)} r_{\text{rdr}} \right] \end{aligned} \right] \quad (14)$$

$$\left[ \rho_{(i,j)}^{\text{air}} C_{p(i,j)}^{\text{air}} v_{c(i,j)}^{\text{air}} A_{c(i,j)} + \frac{2\pi\rho_{(i,j)}^{\text{air}} C_{p(i,j)}^{\text{air}}}{e^{-10^k r_{f(i+1,j)}} - e^{-10^k R_{\text{eff}}}} \int_{r_{f(i+1,j)}}^{R_{\text{eff}}} v_{d(i,j)} \left( \frac{e^{-10^k r_{f(i+1,j)}} - e^{-10^k r}}{2} \right) r_{\text{rdr}} \right]$$

## RESULTS

We present simulation results for five cases: three for polyethylene terephthalate (PET) and two for isotactic polypropylene (iPP). The material properties used for each polymer are listed in *Table I*. Further details about these parameters are in [11]. The algorithm displayed in *Figure 2* is implemented in Matlab [14]. Convergence is reached in 2 or 3 iterations. The code takes less than 30 minutes to execute on a desktop PC.

TABLE I. Material parameters used for simulations.

Name [units]	PET	iPP	
polymer density [g/cm <sup>3</sup> ]	1.36	0.75	
melt shear modulus [Pa]	9.52e4	2.59e4	
surface tension [dyne/cm]	35	36	
$\square_A$ [Pa·s] and $\square_B$ [K] used in Eq. (1)	3.3e4	4.66e3	
ultimate degree of crystallinity [-]	7,570	5,521	
maximum crystallization rate [s <sup>-1</sup> ]	0.42	0.5	
maximum crystallization rate temp. [°C]	0.016	0.55	
crystallization rate curve half-width [°C]	190	65	
	64	60	
	$C_{s1}$ [cal/(g·°C)]	0.2502	0.318
crystalline part	$C_{s2}$ [cal/(g·(°C) <sup>2</sup> )]	0.0007	0.00266
	$C_{s3}$ [cal/(g·(°C) <sup>3</sup> )]	0	0
$C_p$	$C_{l1}$ [cal/(g·°C)]	0.3243	0.502
amorphous part	$C_{l2}$ [cal/(g·(°C) <sup>2</sup> )]	5.65e4	8.0e4
	$C_{l3}$ [cal/(g·(°C) <sup>3</sup> )]	0	0
reference heat of fusion [cal/g]	30	20.1	

For each case, the exponential weight parameter  $k$  used in (14) is set to 4. The parameters governing the spinneret hole spacing are defined in *Figure 6*.

## Simulation 1: Experimental validation

We first compare our results to on-line industry data. Quench air velocity and temperature data were collected at a Wellman, Inc. fiber spinning plant [15].

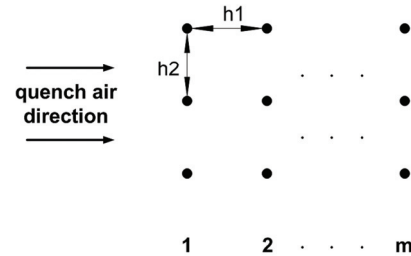


FIGURE 6. Spinneret hole arrangement for simulation.

The spinneret is circular, and the quench air flows from a diffuser in the middle of the spinline (see Jeon and Cox [11] for details). The PET melt is extruded through a spinneret with holes arranged in 10 rings, each containing 300 capillaries. We approximate the hole arrangement as a rectangular array, averaging through the rings. Process conditions, including hole spacings used in the model, are listed in the first column of numbers in *Table II*. The quench profile consists of an active quench zone (0.41 m in length) where air is distributed by the quench diffuser to the fibers, followed by the air entrainment zone (0.43 m long) where the velocity of the quench air was measured as 0.1 m/sec. Speed of the cross-flow quench air on the windward side of the fiber bundle was measured at several points along the spinline.

Table II. Process parameters used for simulations.

Name [units]	PET spinning			iPP spinning	
	Simulation 1: experimental validation	Simulation 2: varying $W$	Simulation 3: high speed	Simulation 4: varying $v_c$	Simulation 5: varying $v_c^{air}$
spinneret temperature [°C]	285	310	310	220	220
mass flow rate [g/min/hole]	0.5231	1.4 & 2.8	2.8	0.7	0.7
capillary diameter [mm]	0.231	0.4	0.4	1.0	1.0
take-up speed [m/min]	1,371	1,200	5,500	1,300 & 2,000	2,000
spinline length [m]	0.8	1.0	1.0	1.5	1.0
upwind air temperature [°C]	35	25	25	25	25
upwind air cross velocity [m/sec]	(see write-up)	0.6	2.0	1.0	0.5, 0.6, & 0.7
quench zone start [m]	0.02	0	0	0	0
quench zone end [m]	0.43	1.0	1.0	1.0	1.0
number of rows	10	10	10	10	10
spinneret length [m]	0.546	0.288	0.288	0.288	0.288
spinneret width [m]	0.03166	0.072	0.01	0.018	0.018
distance between rows [mm]	2.935	7.2	1.0	1.8	1.8
distance between holes [mm]	1.589	3.6	3.6	3.6	3.6

These values are plotted as data points in the first plot in *Figure 7*. A piecewise linear fit of this data, using 3 lines, was used as the inflow condition for quench air in the model. Also shown in the first plot in *Figure 7* are the calculated air cross-velocities in rows 1, 6, and 10. Experimental measurements of quench air temperature on the leeward side of the bundle, at 5 points along the spinline, were also provided. The data points on the leeward side and calculated temperature profiles for rows 1, 6, and 10 are plotted in the second graph in *Figure 7*. The calculated temperatures for row 10 compare well with the experimental data.

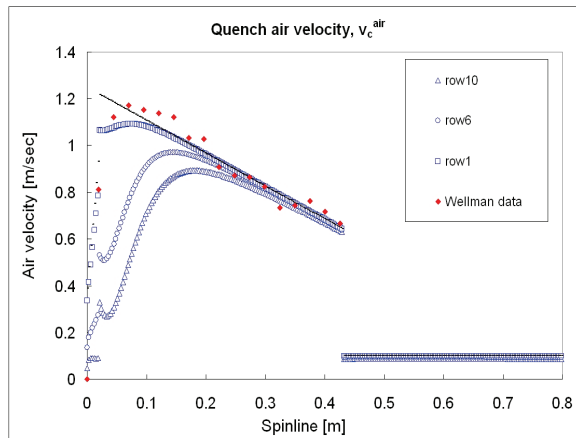
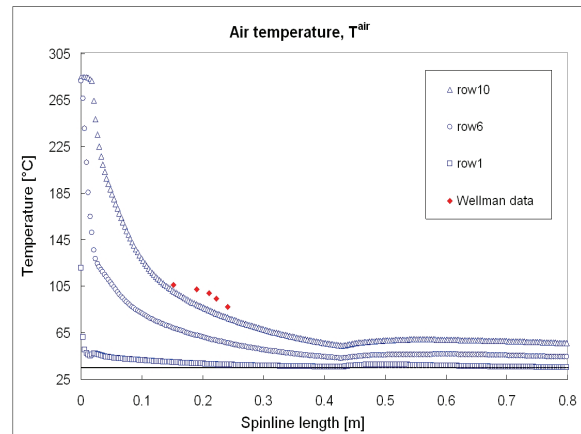


FIGURE 7. Simulation 1 results of quench air velocity and temperature for the Wellman Spinneret at 1,371 m/min take-up velocity: (a) Air temperature,  $T^{air}$  and (b) Air cross velocity,  $v_c^{air}$ .

### Simulation 2: Effects of polymer mass flow rate, $W$

The simulation was used to examine the effects of polymer mass flow rate,  $W$ , for low-speed PET spinning. Process conditions for this simulation are listed in the second column of numbers in *Table II*. Simulation results for fiber speed, temperature, and radius are plotted in *Figure 8*. The variation in quench air conditions between rows resulted in significant variation in fiber characteristics. For the case with the mass flow rate  $W = 1.4$  g/min/hole, the upwind air cross velocity (0.6 m/sec) was sufficient (nearly) to cool the fibers in each row to the ambient (upwind) temperature. When the mass flow rate was raised to 2.8, however, the fibers remained warmer through the spinline likely resulting in more non-uniform final properties. A next step motivated by

these results would be to extend the quench region.

### Simulation 3: High speed PET spinning

In contrast to observations at low speeds, PET fibers spun at higher speeds often exhibit a nontrivial degree of crystallinity. We simulate PET melt-spinning at 5,500 m/min take-up speed and compare computed quantities through the bundle. Process conditions for this simulation are listed in the third column of numbers in *Table II*. The results for fiber speed, crystallinity, and temperature are displayed in *Figure 9*. Warmer conditions from the windward to leeward side resulted in delayed initiation of the velocity plateau, and lower degree of crystallinity on the leeward side.

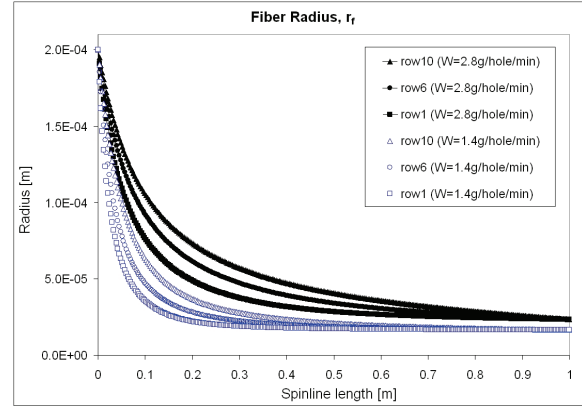
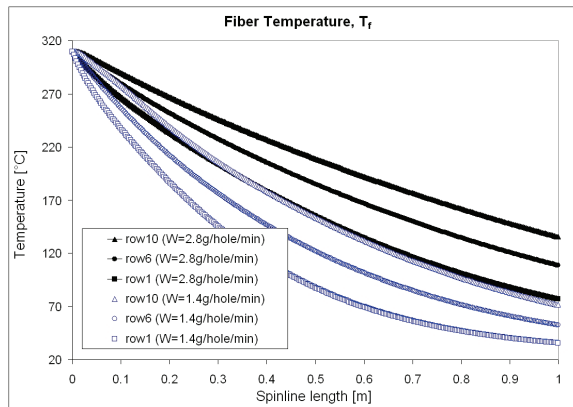
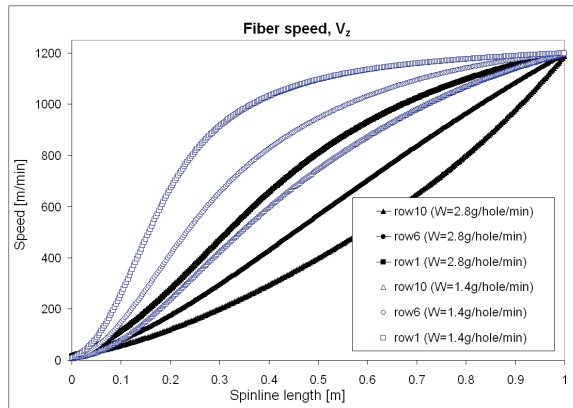
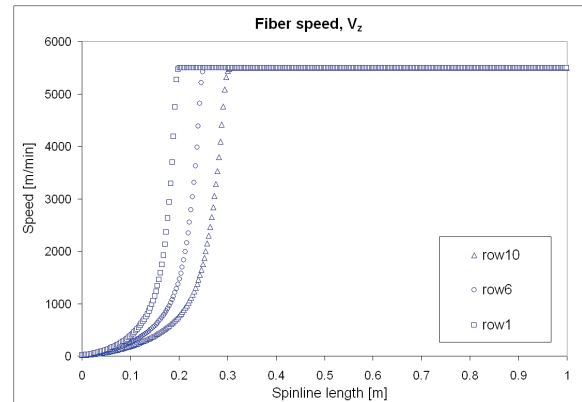


FIGURE 8. Simulation 2 results for fiber properties for different mass flow rates: (a) Take up speed,  $v_z$ , (b) Fiber radius,  $r_f$ , (c) Tensile stress,  $r_f$ , (d) Fiber crystallinity,  $x$ , and (e) Fiber temperature,  $T_f$ .

### Simulation 4: Effects of take-up speed, $v_z$ , for iPP

We investigated the effects of take-up speed for iPP fiber spinning. The process conditions are listed in the fourth column of *Table II*. *Figure 10* contains comparisons of results for take-up speeds of 1300 m/min and 2000m/min. Fiber speed, crystallinity, and temperature are plotted for 3 rows in the bundle. The start of the ‘plateau’ region in the fiber velocity varies from row to row. The final degree of crystallinity in row 1 fibers is more than 10% greater than in row 10 fibers for the 1,300 m/min take-up speed. This result correlates with warmer temperature and lower stress values in row 10 than in row 1. Unlike the spinning results for  $v_z = 1,300$  m/min case, at 2,000 m/min the variation between rows is negligible, likely resulting in more uniform fiber properties. This motivates the consideration of a longer spinline and/or modified quench conditions for lower take-up speeds.



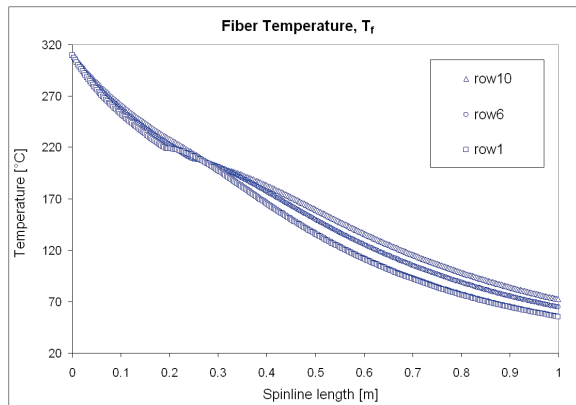
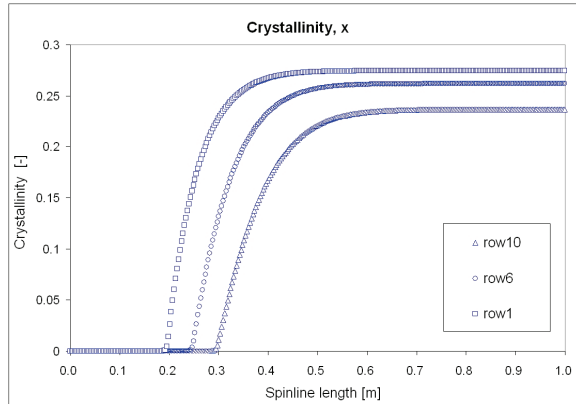


FIGURE 9. Simulation 3 results for PET fiber properties at higher take up speed ( $v_z = 5,500$  m/min): (a) Take up speed,  $v_z$ , (b) Fiber crystallinity,  $x$ , and (c) Fiber temperature,  $T_f$ .

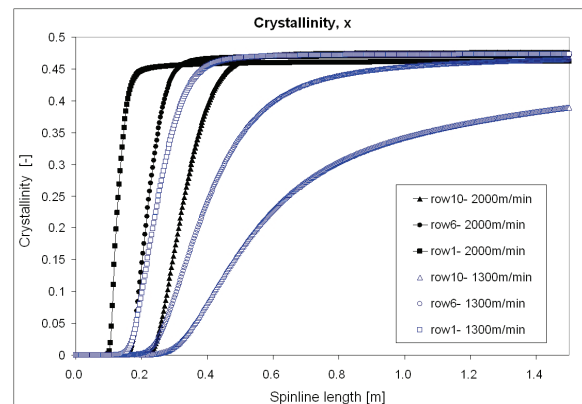
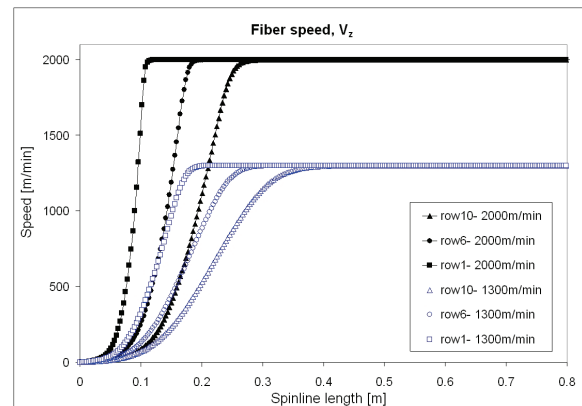
### Simulation 5: Effects of quench air velocity, $v_c^{air}$

We now investigate the effects of varying quench air cross velocity on fiber properties for iPP fiber spinning at 2000 m/min. The process conditions for this simulation are located in the last column of numbers in *Table II*, and the simulation results, (fiber take-up speed, crystallinity, and temperature), are displayed in *Figure 11*. The effect of varying quench air speed is more strongly felt toward the leeward side, especially for degree of crystallinity. This suggests that more non-uniformities in final properties across the bundle may occur at lower quench air speeds. Temperature profiles are shown only for rows 1 and 10 so that the figure is less cluttered.

### CONCLUSIONS

We have presented a versatile melt spinning simulation based on the McHugh et al. FEC single-fiber model and a variation on the multifilament quench zone model of Zhang et al. First we demonstrated the correlation of the quench air

calculation with industry data. Then the code was used to examine trends as material and process properties were varied. Variation of mass flow rate in low speed PET fiber spinning resulted in significant differences in velocity, temperature, and radius profiles. For higher speed PET spinning, a 10% variation in degree of crystallinity is seen between the windward and leeward sides of the bundle. Variation in take-up velocity for iPP fiber spinning showed that fiber properties (notably crystallinity) differed more through the bundle at lower speeds. A similar effect was seen when the inflow quench air velocity was changed, so that at lower air velocity a more drastic variation in fiber properties was seen through the bundle.



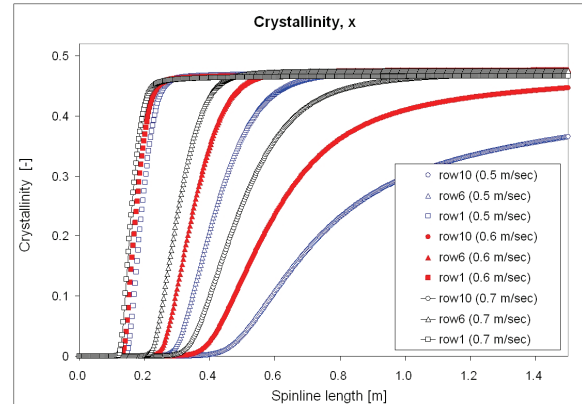
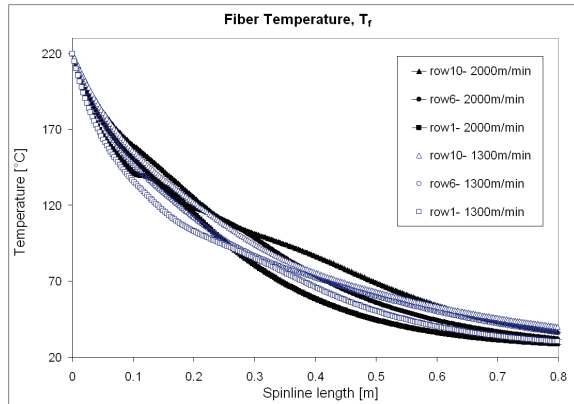


FIGURE 10. Simulation 4 results: comparisons of iPP fiber properties at take-up velocities of 1,300 m/min and 2,000 m/min: (a) Take up speed,  $v_z$ , (b) Fiber crystallinity,  $x$ , and (c) Fiber temperature,  $T_f$ .

Further experimental validation is needed for this simulation. The code will be generalized to model other spinneret geometries, including staggered arrays of capillaries and circular spinnerets. The code will be applied to other polymers at various process conditions. The effects of radiative heat transfer will be incorporated in the simulation, allowing for a study of what process or material conditions warrant the inclusion of both convective and radiative terms.

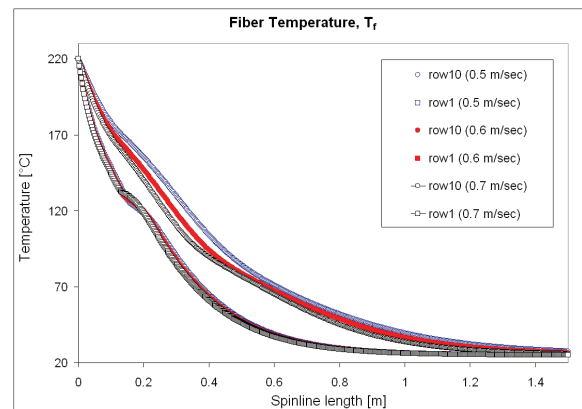
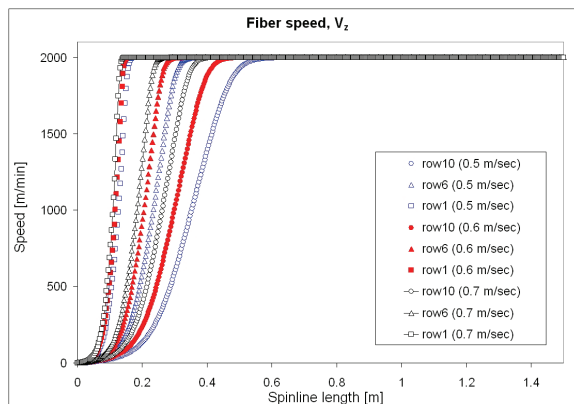


FIGURE 11. Simulation 5: comparisons of iPP spinning results of fiber properties for varying quench air cross velocity,  $v_c^{dir}$ : (a) Take up speed,  $v_z$ , (b) Fiber crystallinity,  $x$ , and (c) Fiber temperature,  $T_f$ .



## ACKNOWLEDGEMENT

This work was supported by the ERC program of the National Science Foundation under Award Number EEC-9731680. The authors gratefully acknowledge Fred Travelute from Wellman Inc. for providing on-line quench air data.

## REFERENCES

- [1] Ziabicki A., Jarecki L., Wasiak A., "Dynamic Modeling of Melt Spinning", *Comput Theor Polym Sci*, 8, 1998, 143-157.
- [2] Denn M.M., *Process Modeling*, Longman/Wiley: New York, 1986.
- [3] Tung L., Ballman R., Nunning W., Everage A., *Computer simulation of commercial melt spinning process*, The Third Pacific Chemical Engineering Congress, 1982, pp. 21-27.

- [4] Dutta A., “Role of Quench Air Profiles in Multifilament Melt Spinning of PET Fibers”, *Text Res J*, 57, 1987, 13-19.
- [5] Zhang C., Wang C., Wang H., Zhang Y., “Multifilament Model of PET Melt Spinning and Prediction of As-spun Fiber's Quality”, *J Macromol Sci Phys*, 46, 2007, 793-806.
- [6] Doufas A.K., McHugh A.J., Miller C., “Simulation of melt spinning including flow-induced crystallization Part I. Model development and predictions”, *J Non-Newt Fluid Mech*, 92, 2000, 27-66.
- [7] Doufas A.K., McHugh A.J., Miller C., Immaneni A., “Simulation of melt spinning including flow-induced crystallization Part II. Quantitative comparisons with industrial spinline data”, *J Non-Newt Fluid Mech*, 92, 2000, 81-103.
- [8] Doufas A.K., McHugh A.J., “Simulation of melt spinning including flow-induced crystallization. Part III. Quantitative comparisons with PET spinline data”, *J Rheol*, 45, 2001, 403-442.
- [9] Shrikhande P., Kohler W. H., McHugh A.J., “A Modified Model and Algorithm for Flow-Enhanced Crystallization—Application to Fiber Spinning”, *J Appl Polym Sci*, 100, 2006, 3240-3254.
- [10] Harvey A.D., Doufas A.K., “Coupled computational fluid dynamics and multifilament fiber-spinning model”, *AIChE J*, 53, 2007, 78-90.
- [11] Jeon Y.-P., Cox C.L., “Modeling of Multifilament PET Fiber Melt-Spinning”, *J Appl Polym Sci*, 110, 2008, 2153-2163.
- [12] Kase S., Matsuo T., “Studies on Melt Spinning. II. Steady-State and Transient Solutions of Fundamental Equations Compared with Experimental Results”, *J Appl Polym Sci*, 11, 1967, 251-287.
- [13] Matsui M., “Air Drag on a Continuous Filament in Melt Spinning”, *Trans Soc Rheol*, 20, 1976, 465-474.
- [14] Matlab, [www.mathworks.com](http://www.mathworks.com)
- [15] Private Communication, Wellman Inc., Charlotte, NC, USA

#### AUTHORS' ADDRESS

**Young-Pyo Jeon; Christopher L. Cox**  
 Mathematical Sciences  
 O-224 Martin Hall  
 Clemson University  
 Clemson, SC 29634-0975  
 USA